# OBSERVING CRUST DEFORMATION ALONG PECENEAGA-CAMENA FAULT

ZLĂGNEAN L., POMERAN M., BEȘUȚIU L.

[1] *Institute of Geodynamics Sabba S. Ștefănescu of the Romanian Academy*

The Baspunar permanent geodynamic station (BGO) is aimed at observing the slip rate along the well-known Peceneaga-Camena Fault (PCF). Its design is based on the idea that intensification of north-westward tectonic push from the Black Sea microplate may reflect in the slip increase along major faults within SE Carpathians foreland. As one of the major faults in the area, changes in the slip rate along PCF may serve as indicator of the increase of tectonic stress with its seismological consequences.
At BGO, two highly accurate Leica TC 1200–1201 total stations (±2ppm accuracy) measure and record every minute the distance between the PCF flanks. Raw observations are then corrected for the influence of atmospheric factors and averaged for a 5 minutes time span. To avoid the effect of fast changes in atmospheric parameters (mainly due to direct hit of the Sun rays), night records are taken into account only. Based on thus corrected and selected observations, slip rate is determined and compared with the amount of seismic energy released.

*Key words:* geodynamics, Peceneaga-Camena fault, Leica TPS 1201 total station, data acquisition software, atmospheric correction, slip rate, seismic energy.

## 1. INTRODUCTION

The Peceneaga Camena Fault (PCF) represents one of the most studied tectonic features of the Romanian territory. Ever since the beginning of the 20th century (e.g., Mrazec 1910, 1912; Macovei, 1912) PCF has been subject of numerous studies regarding its nature, in-depth extent and geodynamic evolution.

During the time, PCF has been considered in many ways, from a local reverse fault (Mrazec 1910; Macovei, 1912), or a large overthrust plane along which Proterozoic Green Schist of Central Dobrogea overthrust Northern Dobrogea Paleozoic deposits (Preda, 1964), to a strike slip fault (e.g., Săndulescu,1980; Hippolyte *et al*. 1996; Hippolyte, 2002).

Geological evidence shows a geodynamic evolution of this fault, with both right-lateral and left-lateral slip episodes (Pavelescu, Nitu, 1977; Săndulescu, 1980; Grădinaru, 1984; 1988; Seghedi, Oaie, 1995; Banks, Robinson, 1997). Scarce crustal earthquakes located on, or near the PCF plane, with strike-slip focal mechanism suggest that the fault might be still active.

It should be stressed that seismic tomography (Martin *et al*., 2006) has revealed PCF as a major lithospheric contact between Moesian Micro-Plate (MoP), and East European Plate (EEP).

Basically, BGO was designed and built up based on the geodynamic model proposed by Beşuţiu and Zugrăvescu (2004), Beșuțiu (2009) to monitor changes in the tectonic stress in the SE Carpathian foreland based on the observation of PCF slip rates.

The appropriate location of the observatory had to satisfy several major conditions like:

- a correct identification of the fault track (based on careful geological/geophysical investigations),
- adequate location on its flanks for emplacing the distance measuring instruments as well as their reflectors; instruments should run in conditions of local stability and best available accuracy,
- secure circumstances for functioning (power supply and backup source, available connection to internet, and permanent guard for observatory devices). All the above-mentioned conditions were encountered in the village of Fântâna Mare, commune of Ciucurova (Tulcea county) where the permanent station was set up (Figure 1).

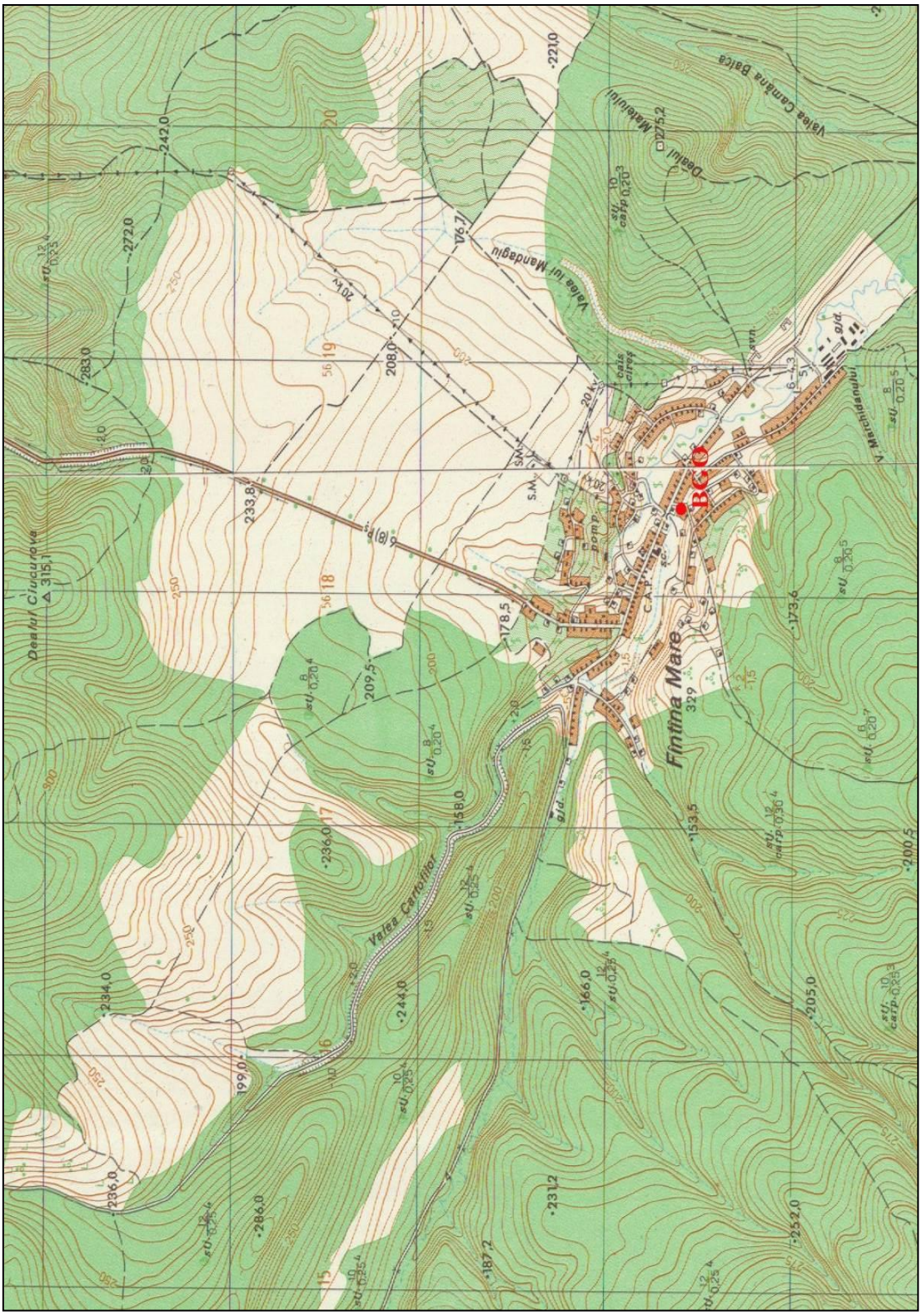


Figure 1 – Location of the Baspunar Permanent Station (BGO). Detail from the topographic map (scale 1:25.000). Approximated coordinates: latitude 44º51'30"N, longitude 28º29'25"E.

## 2. TECHNICAL INFRASTRUCTURE

Two high-precision total stations, Leica TPS 1200 (λ=780 nm) and TPS 1201 (λ= 658 nm) are placed on stable concrete pillars embedded on the southern flank of PCF, in the Proterozoic Green Schists of Central Dobrogea along with a WS2355 weather station for monitoring the atmospheric parameters.

The two total stations point towards two reflectors located on the other side of the fault, on the Jurassic deposits of Northern Dobrogea folded belt, at approximately 300 m (for the reflector placed on the pillar in front of the old school), respectively 350 m (for the reflector located on the wall of the church) (Figure 2).


Figure 2 – The infrastructure of the Baspunar Permanent Station (BGO).

## 3. IMPROVING THE ACCURACY OF DATA ACQUISITION

Leica TPS total stations come from the manufacturer with some internal software for data acquisition aimed at specific precision and speed. Among them, mentions should be made to the **Tracking mode** specialized in fast and continuous monitoring at the expense of precision and the **Standard IR mode** for high-precision measurements which is 3 times more accurate, but 4 times slower than the **Tracking mode**.

Given the peculiarities of the monitoring process, and especially the expected small changes in the fault slip, there has been a need to carry out both continuous observations, and, at the same time, very precise measurements. Therefore, the permanent goal was to improve measurements' conditions and precision continuously and substantially through several ways (such as improving data acquisition or post-processing of time series data).

The increase of data acquisition accuracy was achieved by implementing a new version of acquisition software developed in collaboration with colleagues from the Technical University of Civil Engineering of Bucharest.

The software has been designed and implemented by Dr. Marin Plopeanu from the Faculty of Geodesy and has allowed us to acquire data of high accuracy of the **Standard IR mode** at the speed of the **Tracking mode**.

The software is a stand-alone program, which includes 4 main sections:

1. The connection between the PC and the total station,

2. Command via PC of measurements in Standard IR mode,

3. Execution of repeated code sequences, at the measurement frequency set by the user,

4. Writing the results of observations in external files, easy to be transmitted for processing.

Figure 3 shows the way the data were improved by using the new acquisition software.

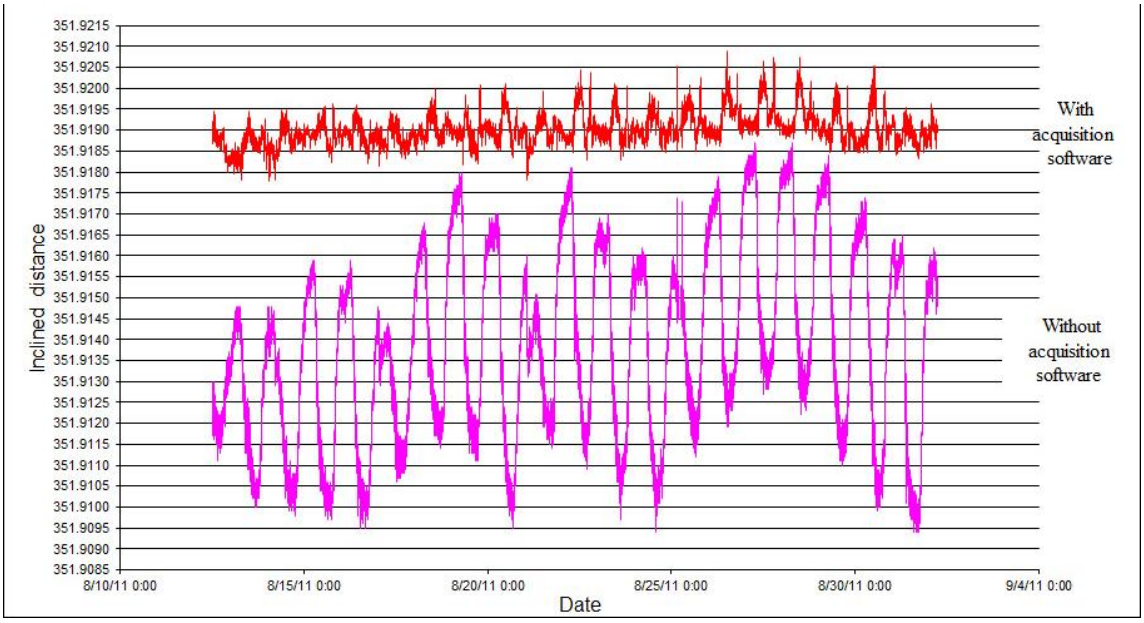


Figure 3 – Data improvement as a result of using the acquisition software.

## 4. DATA POST PROCESSING

Raw data post processing aims to apply some corrections in order to ensure the comparability of the results.

A first measure considered seeks to reduce the influence that atmospheric factors have on geodetic observations and consists in applying specific atmospheric refraction corrections (distances should be corrected for the actual refractive index of air along the measured line, between instrument and reflector). The formulae applied are provided by the manufacturer:

$$S_d corr = (s_d meas \times n0) / n_A$$

where $S_D corr$ is the corrected distance, $S_D meas$ is the measured distance and $n_0$ and $n_A$ have the following forms:

$$n_0 = 1 + \frac{n_g - 1}{1 + 0.003661 * 12} * \frac{760}{760} - \frac{5.5 * 10^{-8}}{1 - 0.003661 * 12} * 4.58 * 10^{\frac{12a}{b+12}} * \frac{60}{100}$$

$$n_A = 1 + \frac{n_g - 1}{1 + 0.003661 * t} * \frac{PmmHg}{760} - \frac{5.5 * 10^{-8}}{1 - 0.003661 * t} * 4.58 * 10^{\frac{at}{b+t}} * \frac{r}{100}$$

$n_g$ is a constant of the instrument we use, in our case Leica Total station models TPS 1200 and TPS 1201 and is provided by the following formula:

$$n_g = 2876.04 + 3 * \frac{16.288}{\lambda^2} + 5 * \frac{0.136}{\lambda^4} 10^{-7} + 1$$

And a=7.5, b= 237.3 and λ = 658 or 780 nm wavelength of the beam (specific for each instrument type).

Other symbols are weather related data at the moment of distance measuring: t[$^o$C] temperature, r [%] relative humidity, $P_{mmHg}$ the absolute pressure

A second measure aimed at removing the influence of the deformations produced by direct solar radiation on the support on which the station's reflector is installed. This deformation is uneven throughout the day depending on the angle of incidence of the sun's rays. For this reason, in studying the dynamics of the Peceneaga-Camena fault (PCF), daily averages and only the nocturnal recordings, between the time of sunset and sunrise, were taken into account.

## 5. DATA POST-PROCESSING SCRIPTS

The idea of developing scripts for processing raw data came from the current trend of increasingly automation within technology. This project started as a learning project for a junior colleague but after many years became a project to whom many people have contributed.

The purpose of the data processing scripts is to automate as much as possible the work needed to transform the field observed data into data corrected by the influence of changes in the atmospheric conditions. The input parameters mainly represent atmospheric factors (air temperature, atmospheric pressure and humidity), and the inclined distance measured between the flanks of the PCF. A full list of the input and output parameters are in Table 1.

The current process of data acquisition involves two human operators, one at the BGO, and the other at the computing center. The field operator is responsible for keeping the hardware in operation and with the daily data transmission to the center. The center operator is responsible for processing the data. All the phases of the process are listed in table 2 and are performed daily (weekdays), Mondays with the data over the week-ends.

Phases 1 and 2 are performed by the field operator. Phase 1 is accomplished by means of the new Laptop 2TPS software previously described. Phases 2 and 3 are facilitated by a well-known web application used to synchronize files across the internet (Dropbox). Phases 3 to 6 are performed by the center operator, some of them being automated. Phase 4 is performed with a click of the mouse and can either process one day or a month, one day at the time. Also, Phase 4 was adapted to run on Windows OS (operating system) with the aid of Vagrant and VirtualBox. Phase 4 consists of a collection of scripts and its sub-phases are described in Table 3.

*Table 1*

Input and output parameters

| # | Type | Role | Description | Observation |
|---|---|---|---|---|
| **1** | Input | Primary | Raw meteo data file | Recorded at 300s intervals |
| **2** | Input | Primary | Raw telemetry data file | Recorded at 300s intervals |
| **3** | Input | Primary | Formulae and their parameters | |
| **4** | Input | Secondary | Current date | From the running computer |
| **5** | Input | Secondary | Date of processed day/month | One month interval |
| **6** | Input | Secondary | Raw files path on the processing computer's file system | Dropbox; rarely changed |
| **7** | Input | Secondary | Output files path on the processing computer's file system | |
| **8** | Input | Secondary | Raw files naming pattern | Human operator names files |
| **9** | Input | Secondary | Timestamps format inside the raw files | |
| **10** | Input | Secondary | Number of seconds needed to shift the time stamps by | Human operator records interval |
| **11** | Input | Secondary | Processed file: raw meteo and telemetry data along with corrected distance | Each record at predefined timestamp 300s apart from the next/previous: 00:00, 00:05, etc. regardless of inherent input data drift |

*Table 2*

Phases in which raw data are transformed into meaningful data

| | Description | Running OS | Observation |
|---|---|---|---|
| Phase 1 | Input records are assembled in files | Windows | automatic |
| Phase 2 | Input files are uploaded in the cloud | Windows | human operator |
| Phase 3 | Input files are downloaded from the cloud | Windows or Linux | automatic |
| Phase 4 | Processing raw data for a range of days | Linux | automatic; can be Linux guest on Windows host |
| Phase 5 | Diurnal data filtered put from phase 4 processed files; compute medians, regression slope | Windows | human operator; MS Excel |
| Phase 6 | Phase 5 medians, regression slope stored as single record for the sunset date | Windows | human operator; MS Excel |

*Table 3*

Automated steps of data processing

| | Description | Observation |
|---|---|---|
| Phase 4.1 | Create folders for the processed day | |
| Phase 4.2 | Prepare input files for the processing scripts | |
| Phase 4.3 | Compensate for hardware clocks drifting apart by shifting the records of one file | |
| Phase 4.4 | Edit the processing scripts to work on the processed day | |
| Phase 4.5 | Extract the data relevant to the processed day | |
| Phase 4.6 | Synchronize records to exact 300s intervals by approximation | |
| Phase 4.7 | Records the lack data, are replaced with only timestamps | Useful for phase 5 |
| Phase 4.8 | Reorder the columns | |
| Phase 4.9 | Apply the formulae and write the output | Output file is in the folder from phase 4.1 |

After applying the atmospheric correction formulae in phase 4, diurnal data is discarded and the night records are mediated in phase 5. All the nocturnal data is condensed in a single record in phase 6.

Phases 4.1 and 4.2 mainly prepare the data and populate secondary input variables (table 1). Phase 4.3 is an application (Pomeran, 2022) designed to compensate if the hardware clocks of weather station and Total station drift apart. Phases 4.4, 4.5, 4.8 and 4.9 are remnant from the early days and the respective code required minimal maintenance. Phases 4.6 and 4.7 were developed later and make use of the generic mapping tools (Wessel, P. *et al*., 2019). It may seem that phases 4.3 and 4.6 are redundant but in the later phase is assumed that the time stamps of the input files are synchronized. The work on these scripts continues, as software bugs occasionally appear, also its goal is not yet achieved.

Figure 4 shows improvement of results after data processing following the above-mentioned listed steps.

## 6. SOME RESULTS

We currently benefit from continuity in monitoring the dynamics of the Peceneaga-Camena fault for about a decade. Figures 5 to 13 show variation of the corrected and daily averaged slope distances between the PCF flanks versus atmospheric parameters recorded at BGO.

There is an overlap of both daily and seasonal variations of the considered parameters (especially temperature). After processing, most of the effects of daily and seasonal variations of the atmospheric parameters are removed from our recordings.

The averaged slope distance variations show a behavior of strike slip type with alternating episodes of the fault sliding. The problem that we posed first and foremost was whether through all the actions that we undertook and that we previously presented, we managed to eliminate the influence of atmospheric parameters, and here we are referring in particular to the temperature, the most influential factor. From the following graphs (Figure 14) it can be seen that a direct, clear connection cannot be established between the corrected slope distances and temperature

variations, so we can appreciate that recorded variations are mostly due to geodynamic causes (Figure 14).

Another question we asked ourselves when BGO was founded, was whether and to what extent there is a connection between the possible sliding on the PCF and the seismic activity in the foreland of the Carpathians arc bend.

Figure 15 shows the earthquakes epicenters of the Vrancea seismic zone and of the Carpathian foreland between 2014 and 2022. Black dots are the epicenters of crustal earthquakes and the red ones of intermediate earthquakes (Figure 15).

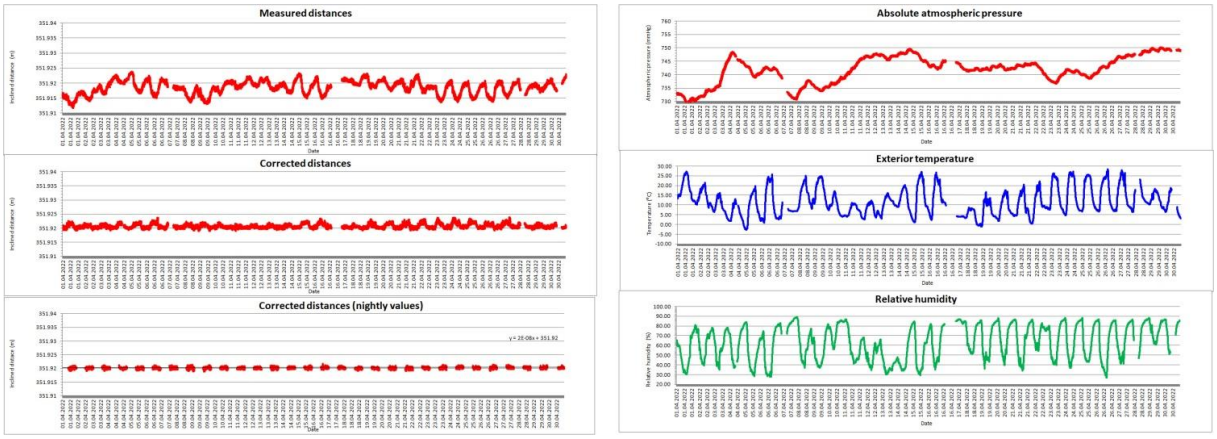


Figure 4 – Measured/corrected distances (left) *versus* atmospheric parameters (right).

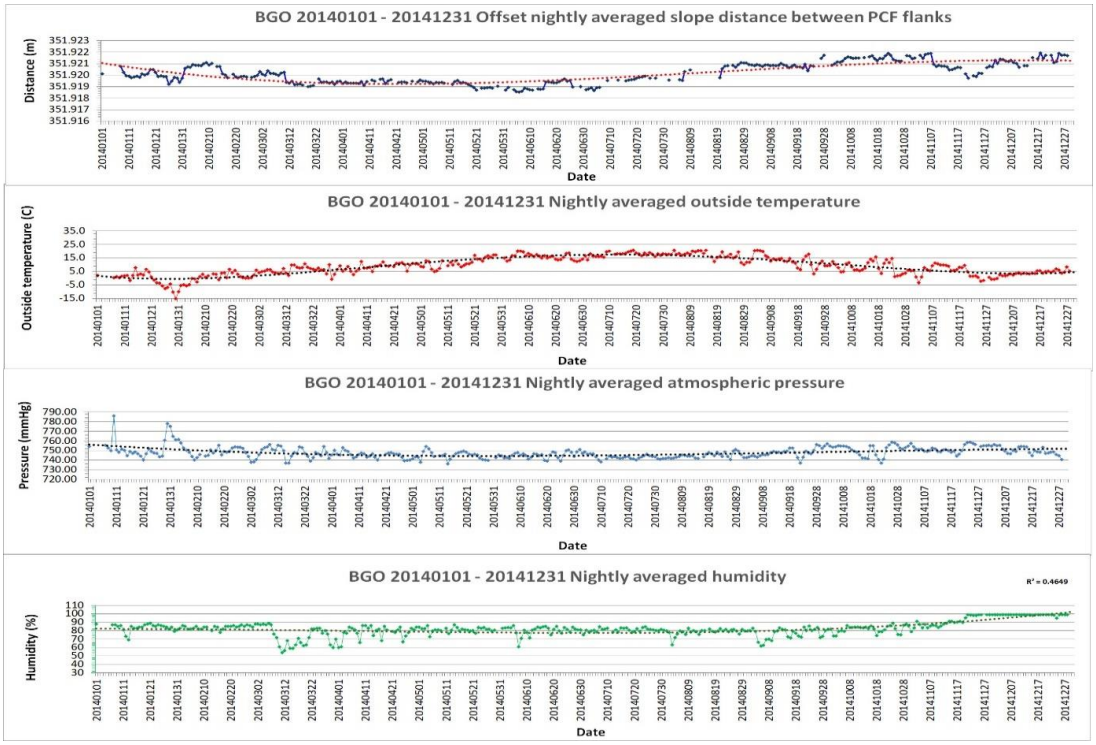


Figure 5 – 2014 Offset nightly averaged slope distance between PCF flanks *versus* nightly averaged atmospheric parameters.

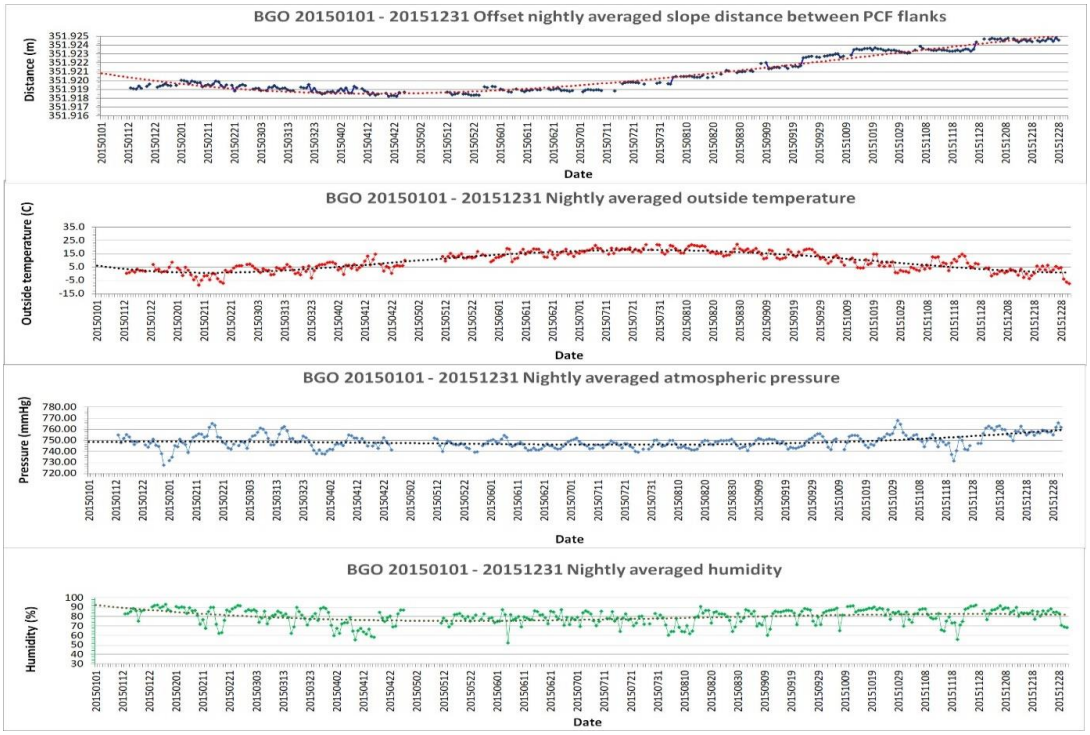


Figure 6 – 2015 Offset nightly averaged slope distance between PCF flanks *versus* nightly averaged atmospheric parameters.

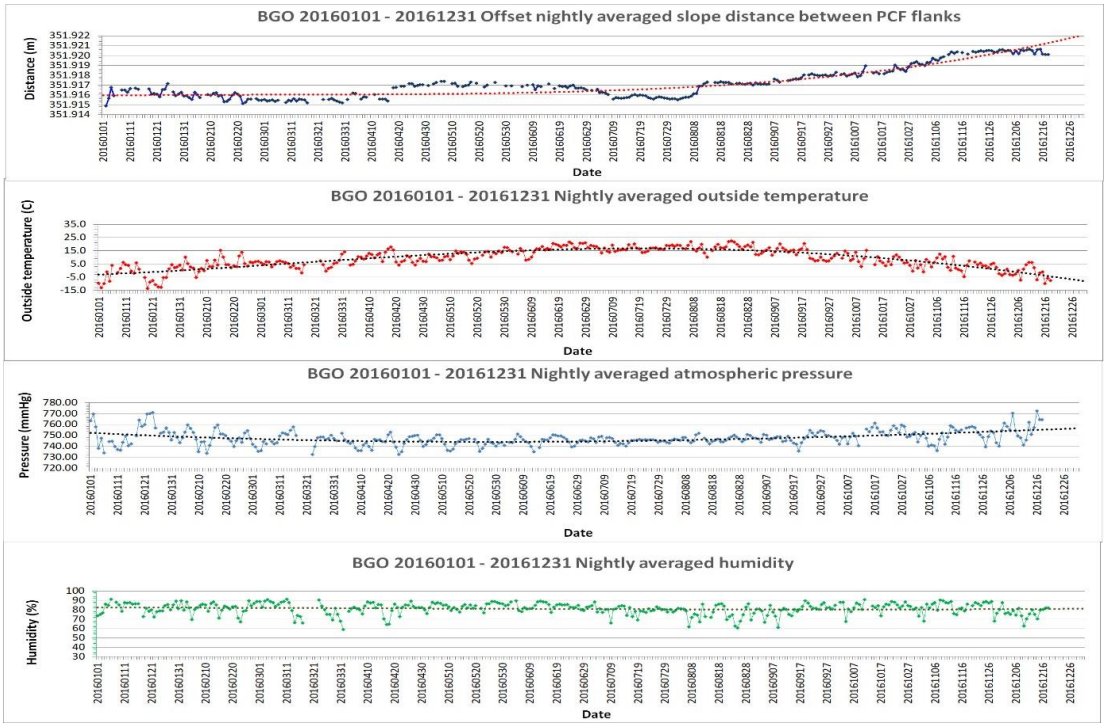


Figure 7 – 2016 Offset nightly averaged slope distance between PCF flanks *versus* nightly averaged atmospheric parameters.

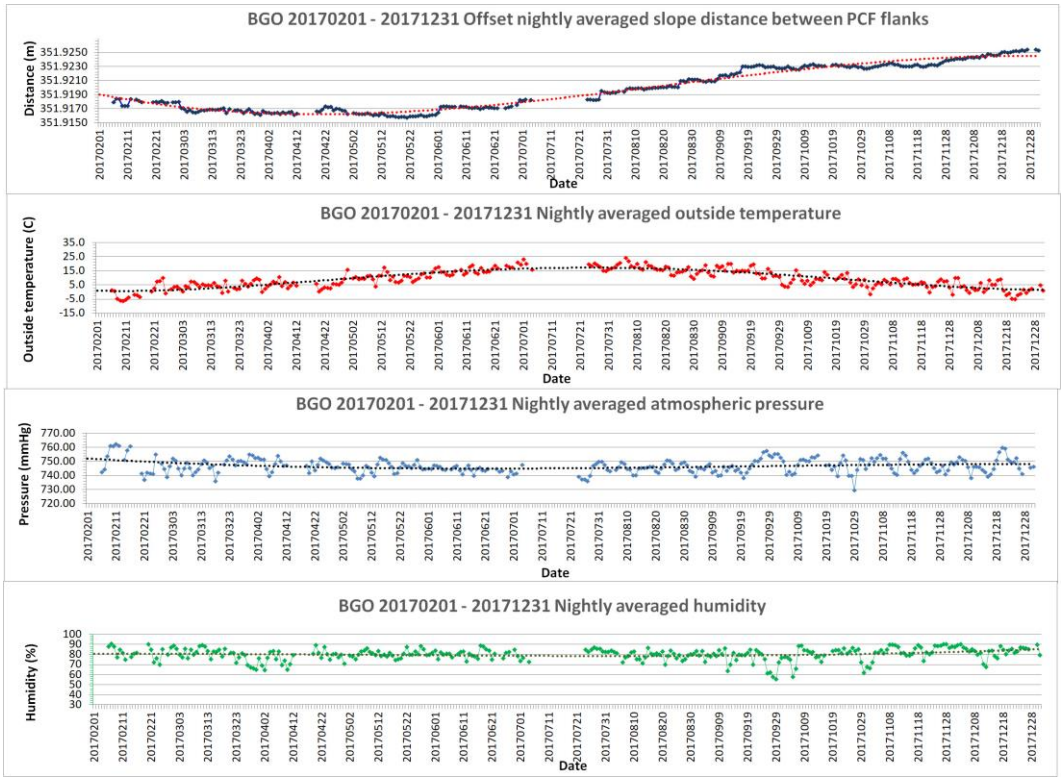


Figure 8 – 2017 Offset nightly averaged slope distance between PCF flanks *versus* nightly averaged atmospheric parameters.

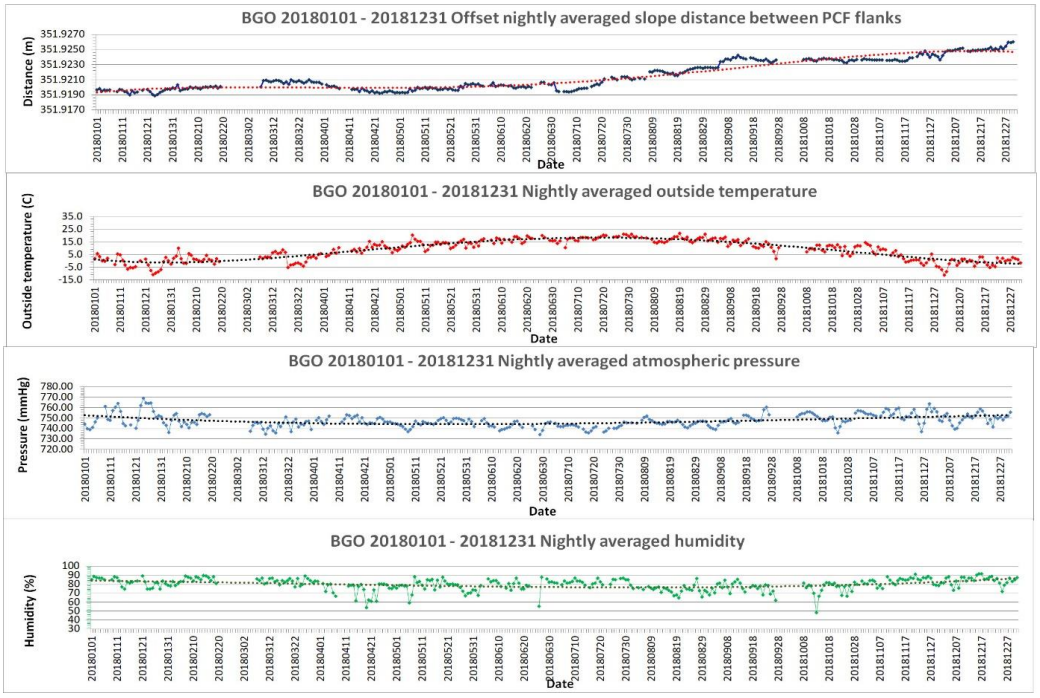


Figure 9 – 2018 Offset nightly averaged slope distance between PCF flanks *versus* nightly averaged atmospheric parameters.

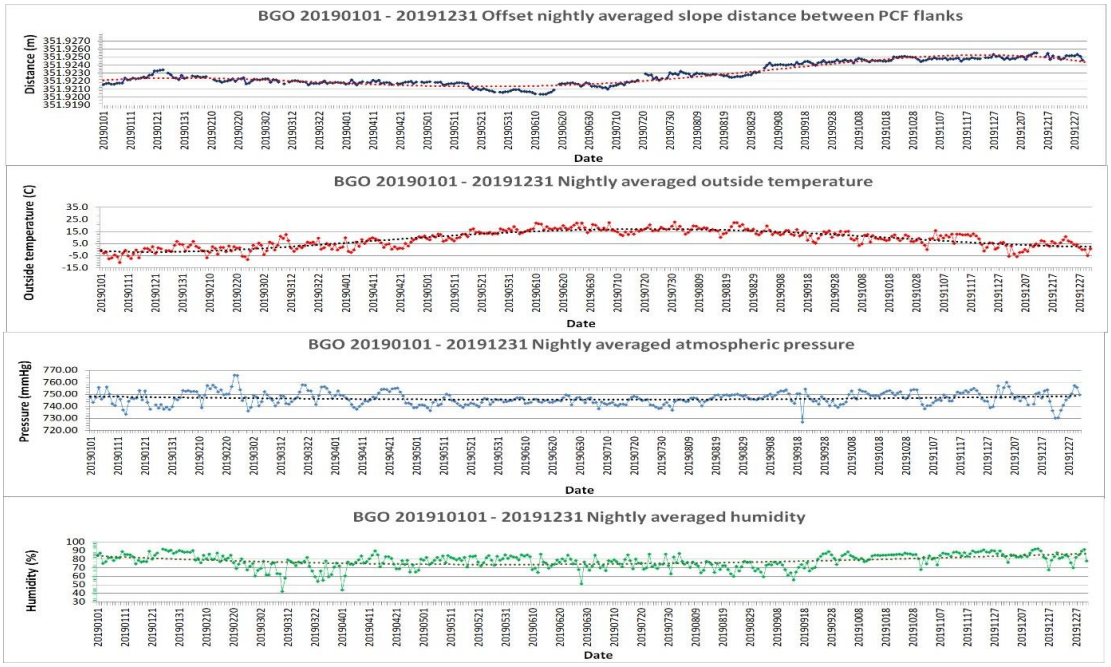


Figure 10 – 2019 Offset nightly averaged slope distance between PCF flanks *versus* nightly averaged atmospheric parameters.


Figure 11 – 2020 Offset nightly averaged slope distance between PCF flanks *versus* nightly averaged atmospheric parameters.

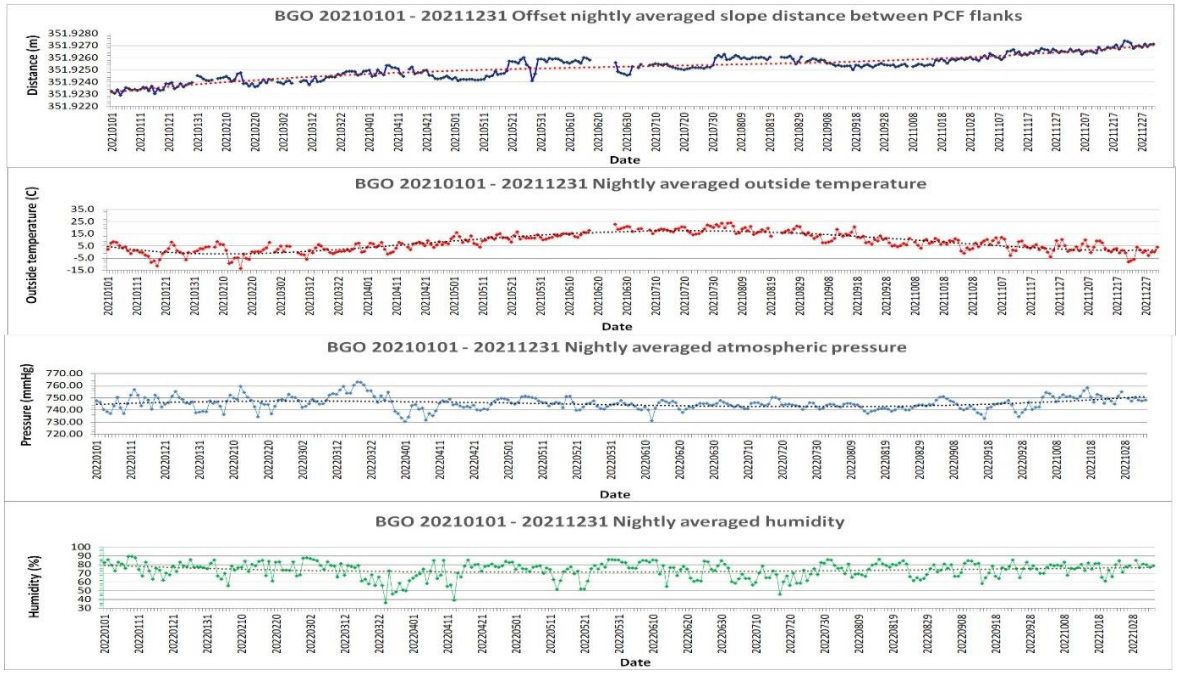


Figure 12 – 2021 Offset nightly averaged slope distance between PCF flanks versus nightly averaged atmospheric parameters.

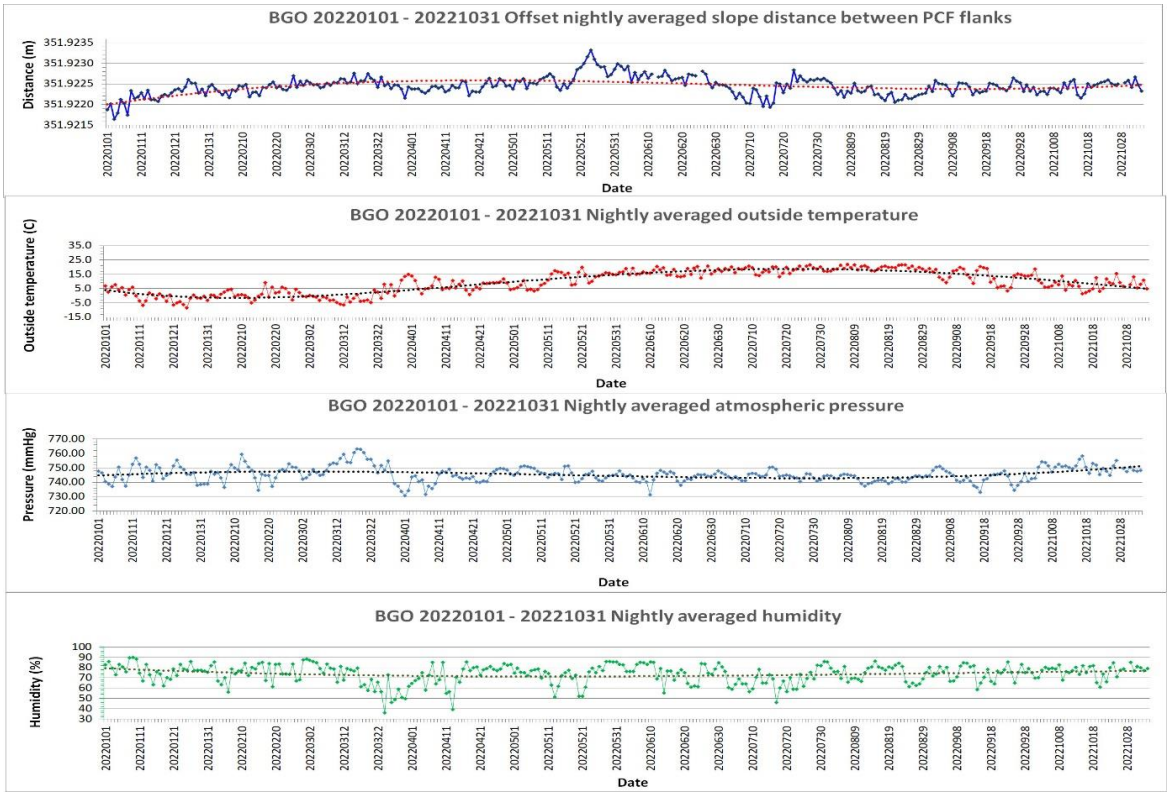


Figure 13 – 2022 Offset nightly averaged slope distance between PCF flanks *versus* nightly averaged atmospheric parameters.

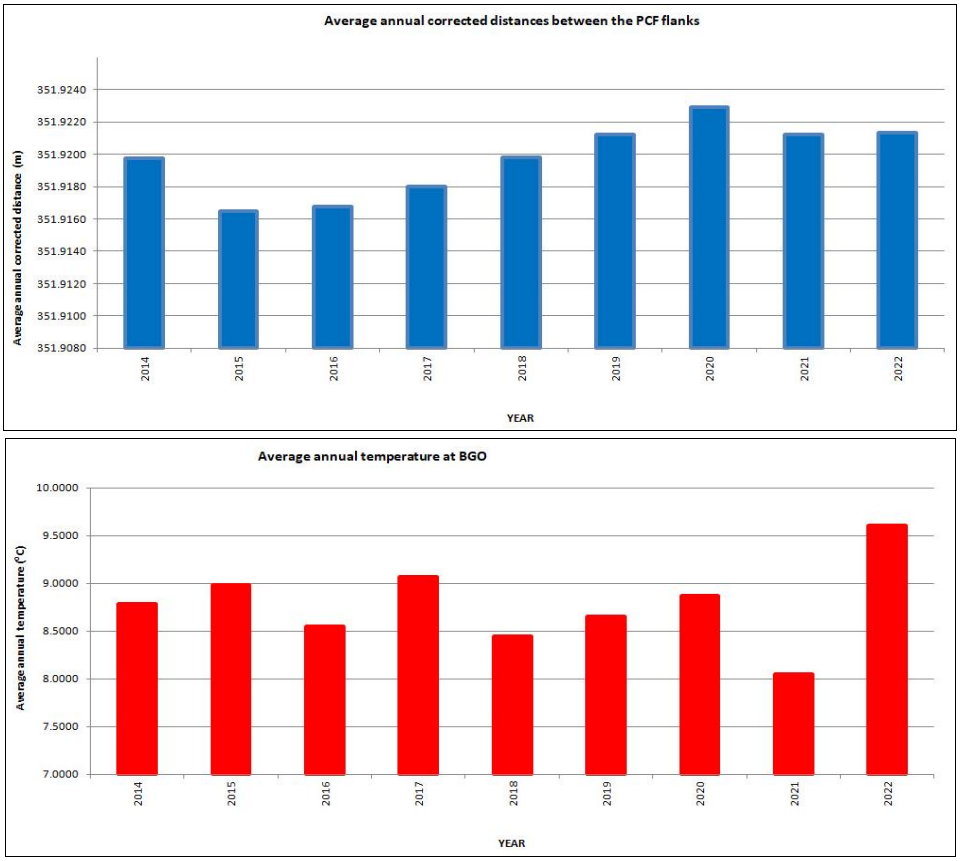


Figure 14 – Average annual corrected distances *versus* average annual temperature recorded at BGO.

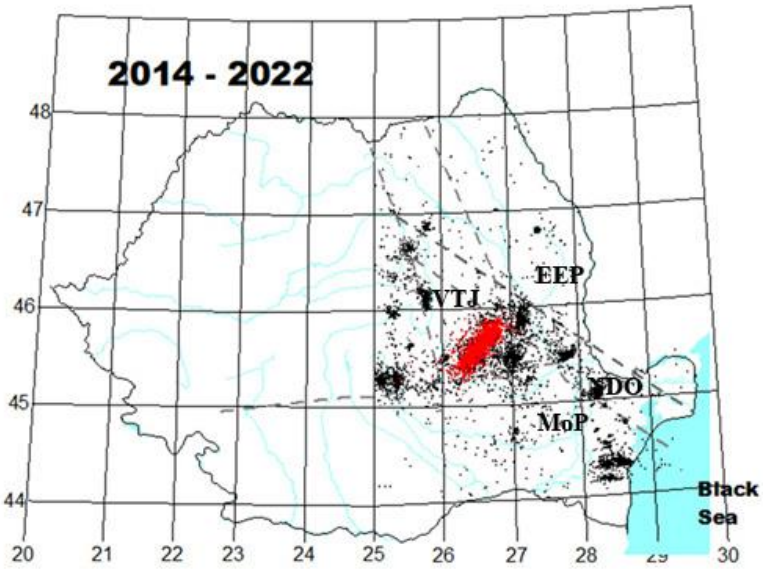


Figure 15 – Seismicity recorded within the Carpathian Bending Arc and its foreland. VTJ-Vrancea Triple Junction, NDO-North Dobrogean Orogen, MoP-Moesian Plate, EEP-East European Plate (Beșuțiu L.,2009).
Red dots – Vrancea intermediate seismicity, black dots – custal seismicity.

Comparing the seismicity of each of the compartments in front of the Carpathians with the average corrected slope distances (Figures 16 and 17), it seems that the slips on the fault are best correlated with the crustal seismic activity in the northern Dobrogea compartment (NDO).

Last but not least it is worth mentioning one of the most representative cases regarding the behavior of the fault, which was caught in the recordings from 2013, when the Galați Izvoarele swarm of earthquakes occurred, and was previously presented in detail (Bețuțiu *et al*., 2019).

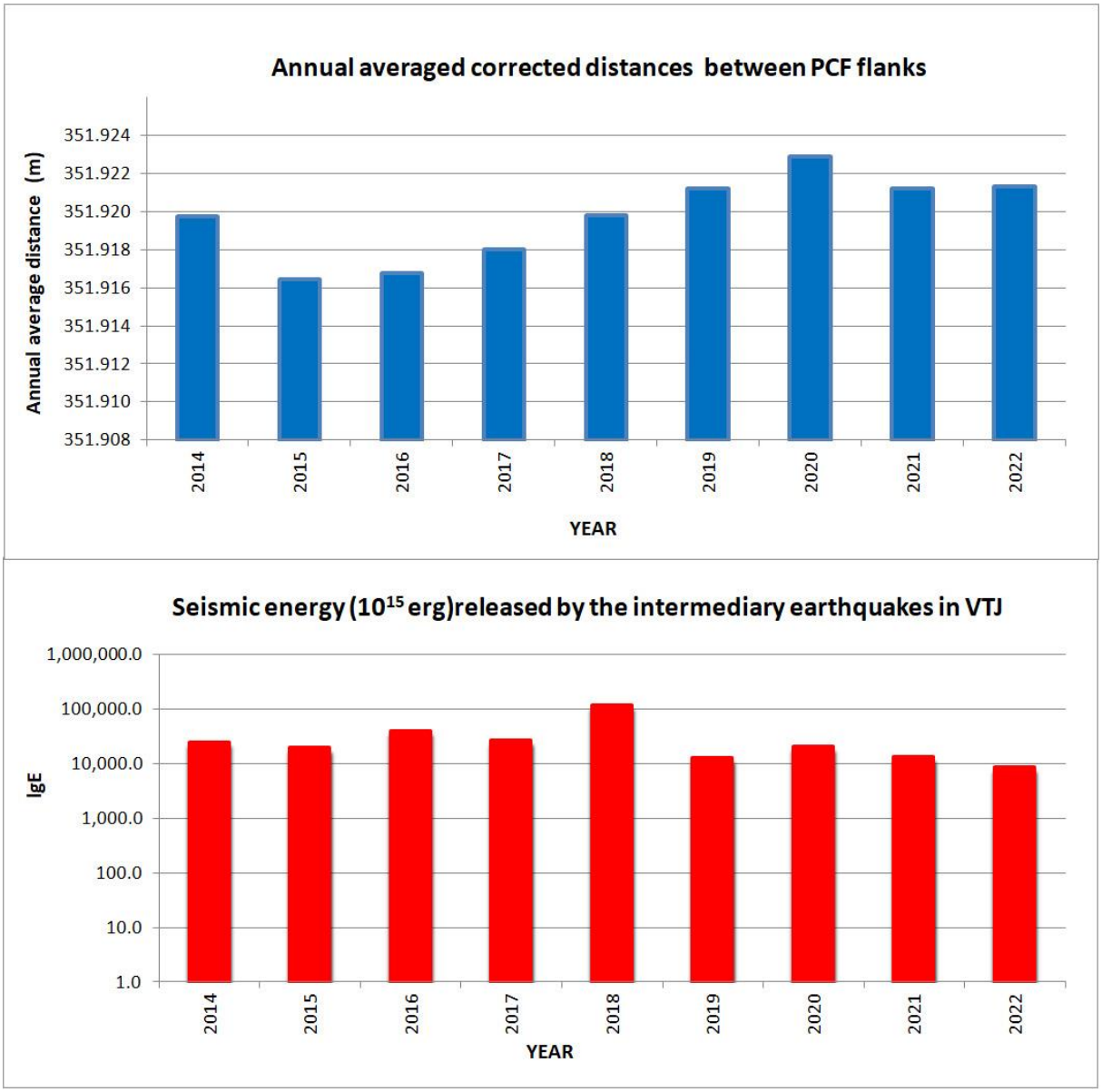


Figure 16 – PCF displacements versus seismic energy released by the intermediary earthquakes in VTJ.

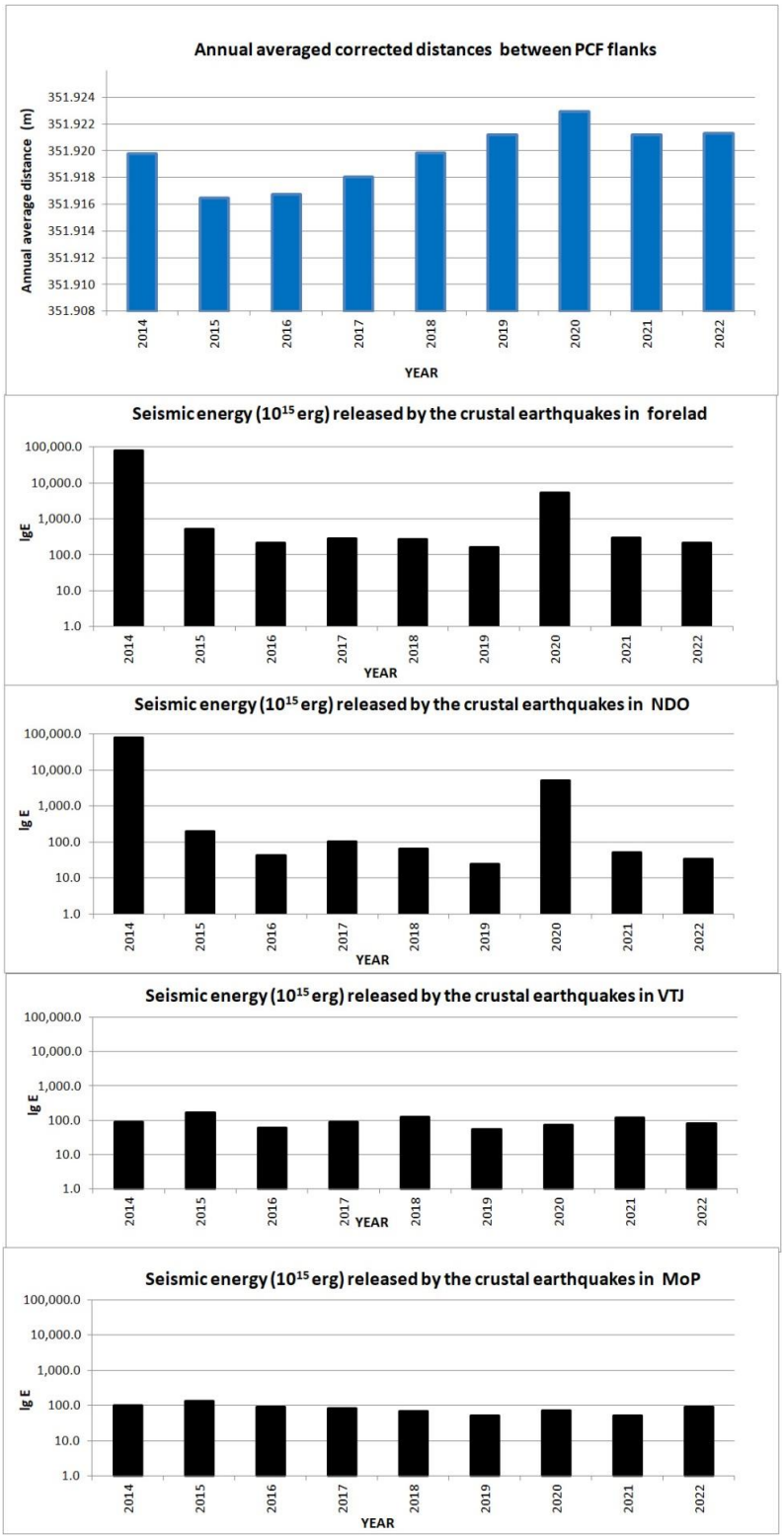


Figure 17 – PCF displacements *versus* seismic energy released by the crustal earthquakes in Carpathian foreland.

REFERENCES

Banks C. J., Robinson A. (1997), *Mesozoic strike-slip back-arc basins of the western Black Sea region*. In A. G. Robinson (Ed.), Regional and petroleum geology of the Black Sea and surrounding region (Vol. 68, p. 53–62). Tulsa: AAPG Memoir

Beșuțiu L., Zugrăvescu D. (2004), *Considerations on the Black Sea opening and related geodynamic echoes in its NW inland as inferred from geophysical data interpretation*. Ukrainian Geologist, no.3, p. 51–60, Kiev.

Beșuțiu L. (2009), *Geodynamic and seismotectonic setting of the SE Carpathians and their foreland*. In: L. Beșuțiu (Ed.) Integrated research on the intermediate depth earthquakes genesis within Vrancea zone. Vergiliu Publ. House, p. 233–248.

Beșuțiu L., Diaconescu M., Zlăgnean L., Craiu A. (2019). *Structural and Geodynamic Ideas on the Galati-Izvoarele Seismic-Prone Area (Eastern Romania)*. Pure Appl. Geophys. **176,** 65–95, https://doi.org/10.1007/s00024-018-1956-0

Grădinaru E. (1984) - *Jurassic rocks of north Dobrogea. A depositional–tectonic approach*. Rev. Roum. Géol., Géophys. Géogr., 28, 61–72.

Grădinaru E. (1988), *Jurassic sedimentary rocks and bimodal volcanics of the Carjelari-Camena outcrop belt: evidence for a transtensile regime of the Peceneaga-Camena Fault*. Stud. Cerc. Geol., Geofiz. Geogr., Ser., Geol., Acad. Române, 33, 97–121, Bucharest.

Hippolyte J.C., Săndulescu M., Bădescu D., Bădescu N. (1996), *L'activité d'un segment de la ligne Tornquist-Teisseyre depuis le Jurassique superieur: la faille de Peceneaga-Camena (Roumanie)*. Comptes Rendus de l'Academie des Sciences Paris, Serie II. Sciences de la Terre et des Planetes, 323:1043–1050.

Hippolyte J.C. (2002), *Geodynamics of Dobrogea (Romania): new constraints on the evolution of the Tornquist–Teisseyre Line, the Black Sea and the Carpathians*, Tectonophysics 357, 33–53.

Martin M., Wenezel F., CALIXTO WORKING GROUP (2006), *High-resolution teleseismic body wave tomography beneath SE-Romania – II, Imaging of a slab detachment scenario*. Geophysical Journal International 164, 579–595.

Mrazec L. (1912), *Asupra liniei de încălecare Peceneaga-Camena* . D.S.Inst. Geol.Rom., III, p. 163–165.

Mrazec L. (1910.), *Distribuirea rocelor verzi în direcțiunea stratelor în care se găsesc*. D.S. Inst. Geol. Rom., II, p. 26–39.

Macovei G. (1912), *Observațiuni asupra liniei de încălecare Peceneaga –Camena*, D.S.Inst.Geol.Rom, III, Bucuresti, p.155-163

Pavelescu L., Nițu G. (1977), *Le probléme de la formation de l'arc carpatho-balkanique*. Ann. Univ. Bucur. Geol. 26, 19–35.

Preda D.M., (1964), *Forelandul carpatic şi poziţia sa tectonică în cadrul structural-geologic al Europei (The Carpathian foreland and its position within the geological-structural setting of Europe)*. An. Com. Geol., XXXIII, (in Romanian) R.S.R., București, p. 9–36.

Sandulescu M.(1980), *Analyse géotectonique des chaînes alpines situées autour de la Mer Noire occidentale*. Ann. Inst. Geol. Geofiz. 56, 5–54, Bucharest.

Seghedi A., Oaie G. (1995), *Palaeozoic evolution of North Dobrogea*. In: Săndulescu *et al*. (Eds), Field Guidebook, Central and North Dobrogea IGCP Project no. 369 Comparative evolution of PeriTethyan Rift Basins, Mamaia , 5–75.

Pomeran M. (2022), *Time shift* (Version 0.0.1) [Computer software].https://doi.org/10.5281/zenodo

Wessel P., Luis J. F., Uieda L., Scharroo R., Wobbe F., Smith W. H. F., Tian D. (2019), *The Generic Mapping Tools version 6*. Geochemistry, Geophysics, Geosystems, 20, 5556–5564. https://doi.org/10.1029/2019GC008515

*** – Leica TPS 1200 and 1201 User Manuals.